

Look Closer to Your Enemy: Learning to Attack via Teacher-student Mimicking

Mingjie Wang

Guangdong Key Lab of AI
and Multi-Modal Data Processing,
BNU-HKBU United International College
mjwang0606@gmail.com

Zhiqing Tang

Institute of Artificial Intelligence
and Future Networks,
Beijing Normal University
domain@sjtu.edu.cn

Sirui Li

Guangdong Key Lab of AI
and Multi-Modal Data Processing,
BNU-HKBU United International College
p930026068@mail.uic.edu.cn

Dingwen Xiao

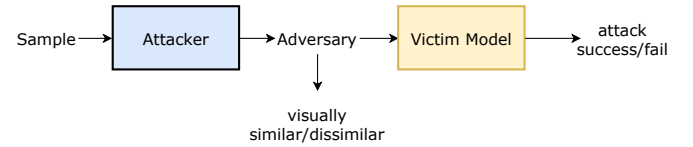
Guangdong Key Lab of AI
and Multi-Modal Data Processing,
BNU-HKBU United International College
p930026130@mail.uic.edu.cn

Abstract—Existing adversarial attack methods mainly focus on generating attack samples via the misclassification supervision feedback of victim models (VM), while little attention is paid to what the VM really believes. This paper aims to generate realistic attack samples of person re-identification (ReID) by reading the enemy’s mind (VM). Three inherent benefits could be uncovered: (1) Directly leveraging VM’s knowledge to attack is transferable to test set in open-set ReID. (2) Cheating the belief of VM could mislead it easier. (3) Since VM only remembers the clean images, cheating their minds could boost the attack image generation to be realistic and undetectable. However, how to read VM’s mind and then cheat it is intractable. In this paper, we propose a novel inconspicuous and controllable ReID attack baseline, LCYE (*Look Closer to Your Enemy*), to generate adversarial query images. Concretely, LCYE first distills VM’s knowledge via teacher-student memory mimicking in the proxy task. Then this knowledge prior acts as an explicit cipher conveying what is essential and realistic, believed by VM, for accurate adversarial misleading. Besides, benefiting from the multiple opposing task framework of LCYE, we further investigate the interpretability and generalization of ReID models from the view of the adversarial attack, including cross-domain adaption, cross-model consensus, and online learning process. Extensive experiments on four ReID benchmarks show that our method outperforms other state-of-the-art attackers with a large margin in white-box, black-box, and target attacks. Our code is now available at <https://gitfront.io/r/user-3704489/mKXusqDT4ffr/LCYE/>

I. INTRODUCTION

Person re-identification (ReID) [1]–[8] aims to associate images of a person across disjoint cameras. Recently, deep learning-based methods [2] even achieved over 90% Rank1 accuracy and surpassed human-level performance. However, deep ReID models are found to be vulnerable to the adversarial examples, i.e., minor perturbation in original examples could

Standard Attack Paradigm



Our Look Closer to Your Enemy

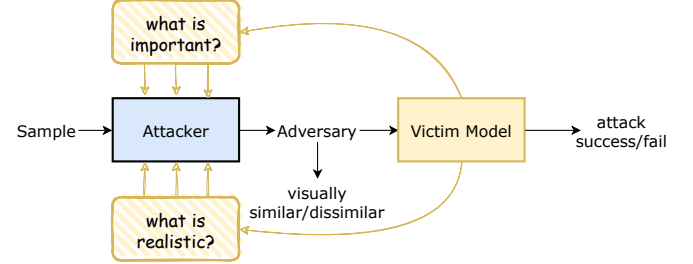


Fig. 1: Illustration of standard attack paradigm and our *Look Closer to Your Enemy*.

mislead the model to mistake with a high confidence [9]. In this paper, we investigate building an efficient adversarial attacker to generate more aggressive but human-imperceptible noise by reading the victim model’s (VM’s) mind.

For attacking image retrieval models, current studies [9], [10] mainly borrow the paradigm from classification attack **deepfool**. As shown in Figure 1, under the supervision for attack and imperceptible purposes, the attacker gradually optimizes toward a stable status between this tradeoff. However, we believe this paradigm is suboptimal. (1) It lacks pixel-level guidance considering both attack and imperception, since attack supervision gives a global feedback. (2) The VMs of recognition task are trained by classification loss and attacked by misclassification loss, which is consistent. However, ReID VMs are trained with different structures and losses, e.g., PCB [11] and circle loss [12], while attacked by the similar global

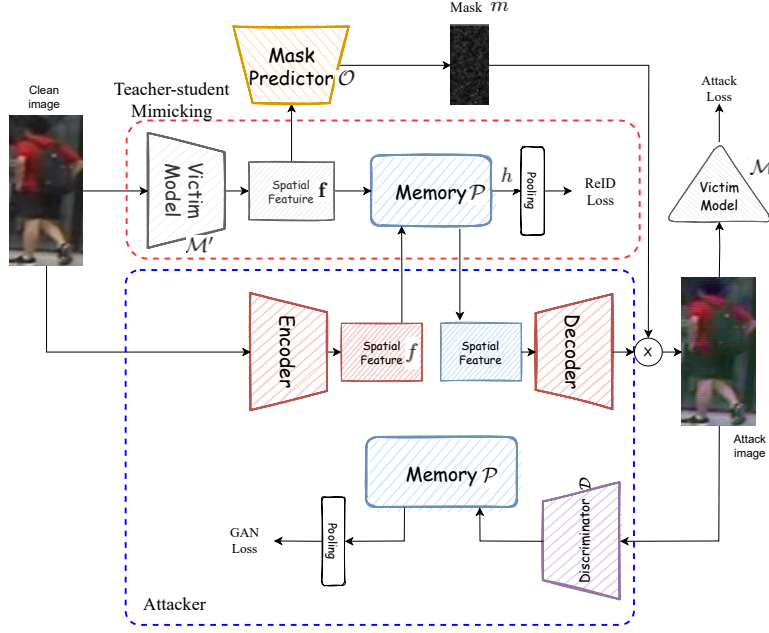


Fig. 2: The unrolled framework of our *Look Closer to Your Enemy*(LCYE). The generator \mathcal{G} of attacker has an encoder and a decoder which retrieves relevant prototypes from memory module \mathcal{P} at the middle of encoder-decoder.

misranking loss. (3) The adversarial identity consistency for personalized and realistic generation is not guaranteed in both RGB and latent space in GAN-based attacker [9] where the discriminator only tells real/fake instead of belonging to the attended identity.

In this paper, to escape the optimization curses, we step further to cheat VM’s mind to attack. This idea is similar to ‘*attack your enemy in his own way*’. For example, the attacker could erase the region trusted as the true identity by VM and add the region trusted to another identity. Therefore, one reasonable solution is to cheat the pixel-level decision-making process of VM, since it remembers what a real image is and what determines an image to the specific identity. This manner could bring three-fold benefits: (1) The attacker could be transferable to a cross-domain test set, since the knowledge of well-posed VM is naturally transferable. (2) It provides pixel-level guidance taking into account both realistic and harmful generation for the attack. (3) Cheating VM’s mind alleviates the necessity of overturning VM during training to obtain enough negative feedback.

Accessing the decision-making process of VM is easy. However, how to leverage it to attack is not. It is decomposed into two steps, *i.e.*, recording the belief of VM and searching for a similar but wrong potential target for attack. One related method is [13] that stores the latent feature of all images of a VM-like model in a memory bank and then search the nearest potential target belonging to another category. Nevertheless, the search complexity is square to the total image number and the final generation could not be guaranteed and reasonable, *e.g.*, forcing a man to have long hair and wear a dress.

In this paper, we propose a novel inconspicuous and controllable attack baseline using VM’s identity-level mind. Note that humans may not remember what a person looks

like but remember a general prototype about him hidden in cognition. One explicit example is the attribute of each person, like ‘*a young man wears a yellow shirt, black pants, and a hat without a bag*’, provided by Market1501 [14] and DukeMTMC [15]. The attribute is a concrete instantiation. In this paper, we aim to cheat VM’s unconscious belief. Inspired by this observation, instead of searching for an instance-level accurate image, *i.e.*, forcing one image to generate as another image, we advocate to searching for a general identity-level structural prototype, which is believed by VM, to generate. As shown in Figure 2, we first record VM’s mind by proposed attention-like memory module via teacher-student mimicking and then let the attacker retrieve the potential target prototype from it via ensuring preservation consistency. Specifically, the knowledge of what VM believes identity is online learned and recorded in the parameterized memory module. Then, both the generator and discriminator retrieve relevant prototypes by reading the memory for different goals: the generator retrieves the prototype of potential targets for the attack. In contrast, the identity-wise discriminator checks whether the generated image preserves the prototype of the target identity. We unify, we unify the pixel-level attack and perception measurement within a preservation-consistent GAN.

Another contribution of this work is investigating the interpretability and generalization of ReID models from the view of the adversarial attack, including cross-domain adaption, cross-model consensus, and the online learning process. The independent teacher and student model in mimicking branch bring the convenience of analyzing explainable ReID with various hybrid combinations. Although numerous papers [16] focus on these concerns, our method could jointly delve deep into all of them. Therefore, our contributions could be summarized as follows:

- (1) We propose a novel ReID attack baseline named *Look*

Closer to Your Enemy (LCYE) to solve the issues from joint attack & imperceptibility optimization.

(2) We delve deep in interpretable and generalizable ReID from the aspect of adversarial attack by evaluating model consensus, covering cross-model&cross-domain covariance and online learning process.

(3) Our method obtains a promising attack success rate with inconspicuous noise. Experimental validations on four of the most extensive ReID benchmarks with both CNN and Transformer-based ReID SOTAs [2], [11] validate our method’s superior efficiency and transferability in white-box, black-box, and target attacks.

II. RELATED WORK

Person Re-identification aims to spot the appearance of the same person in different observations [12]. Deep feature-based methods [17]–[20] and metric learning-based methods [21]–[23] have achieved significant progress in supervised ReID.

For deep feature-based methods, a cascade structure has already been studied in the neural network literature in the 1980s [24]. Although fully connected cascade networks trained with batch gradient descent [25] are effective on small datasets, this method only applies to networks with a few hundred parameters. In [26]–[29], it has been found to be effective for various vision tasks to utilize multi-level features in CNNs through skip-connections. Then, the pure theoretical framework of networks with cross-layer connections is derived [30]. Highway Networks was the first batch of architectures that provided effective training methods for more than 100 layers of end-to-end networks [31].

Additionally, ResNets have achieved impressive performance like ImageNet and COCO object detection [32]. ResNets with pre-activation can also help train state-of-the-art networks with more than 1000 layers [33]. For metric learning-based methods, TriNet [34] samples the most negative samples in the batch to achieve rapid convergence. The negative samples were found by Harwood et al. [35] from the increasing search space defined by the nearest neighbor distance. For example, TransReID [2] achieves state-of-the-art performance with the participation of local-aware Transformer [36]. Moreover, other innovative works [16], [37], [38] already focus on the interpretable and generalizable ReID which is verified by improved results. However, these methods may not be suitable and scalable for different tasks and models. In this paper, we aim to jointly analyze different ReID models in the point of supervised and unsupervised adversarial attack, keeping the fairness and flexibility of assessing the robustness and generalization. This attempt is not limited to cross-validation via simple white-box, black-box attack but covers the implicit decision-making.

Adversarial Attack is to extract samples from real data to fool the learning model and help evaluate the robustness of the target models [39]–[41]. The security problems of the current most advanced model [42], [43] and more insights of the CNN mechanism [44] were raised by Szegedy et al. The fast-gradient sign method [44], which generates adversarial examples in one step, is one of the earliest works of gradient-based attack. The primary iterative method [45], deep fool [46]

and iterative momentum method [18] extend the fast-gradient sign method [44] to update the adversarial images with small step sizes iteratively. Score-based attacks rely on searching input space. Single-pixel perturbation out of the valid image range can successfully lead to misclassification on small-scale images [47], which can be extended to large-scale images by local greedy searching. In addition to pixel modification, the adversarial examples can also be resulted in by sample generation via spatial transform [48]. The iterative least-likely class method [45] increases the prediction probability of the least possible class through constraints, so that the classification model outputs interesting errors.

Adversarial Attack on ReID needs to generalize to unseen query images using misranking loss, which is different from adopting misclassification loss in close-set recognition tasks [49], [50]. For optimization-based methods, [51] proposes an ODFA which aims to exploit feature-level adversarial gradients. [10] proposes a metric attack to distort the distance between the attacked image and other similar images. Besides, [9] introduces a GAN-based misranking attacker whose transferability is proved by its post-hoc results. However, these methods still ignore the pixel-level supervision considering both attack and perception, which is essential to tackle their tradeoff. In this paper, we propose our LCYE to solve this issue by cheating VM’s mind to generate harmful but realistic images.

III. METHODOLOGY

A. Problem Setup for ReID Attack

First, given a clean image and its ground truth label (x, y) , the goal of adversarial attack is to lead model \mathcal{M} to misclassify the label of an input x by finding an adversary x' satisfying:

$$\min_{x'} \mathcal{H}(x, x') \quad \text{s.t.} \quad \mathcal{A}(\mathcal{M}(x'), y) \quad (1)$$

where \mathcal{H} and \mathcal{A} are pixel-level perception loss and global-level attack loss, respectively. Thus, it naturally lacks pixel-level supervision considering two purposes jointly. Instead, perception loss \mathcal{H} and adversarial loss \mathcal{A} search the potential adversary x' on RGB and latent space separately. The joint gradient $\partial L = \frac{\partial \mathcal{H}}{\partial x} + \lambda \cdot \frac{\partial \mathcal{A}}{\partial x}$ is intervened by predefined tradeoff factor λ , and the optimization is finally trapped in a local biased optimum.

Second, for close-set recognition tasks where training and test sets share identical categories, VM \mathcal{M} s are trained with cross-entropy loss and attacked by adversarial cross-entropy loss, which is consistent. However, the training of open-set ReID models \mathcal{M} varies in structures and losses, *e.g.*, PCB mines local representation, but \mathcal{M} is unanimously attacked via adversarial triplet loss on global features. This setting omits the characteristic spirit of individual models. One solution is to customize the attack supervision for different models adjustably, but it is arduous.

Third, adversarial category consistency for realistic generation is weak in GAN-based attackers [9], [52]. These methods use the fixed VM as an external category discriminator and additionally learn an online real/fake discriminator to meet the demand of realistic generation. However, the fixed external VM is easy to be fooled by the generator. At the same

time, the naive real/fake discriminator cannot tell the realistic personalized images instead of solely realistic images. We verify this issue in Section IV-A, which shows that attacked images of the GAN-based method have more conspicuous noise.

Essentially, we believe the current paradigm of adversarial attack is more like an adversarial reinforcement trial from VM. These issues are raised from the ignorance of learning from samples and considering what VM believes. In this paper, we propose a novel method named LCYE to solve the issues mentioned above unitedly by cheating the sample-driven decision-making process of VM.

B. Overall Framework

The unrolled framework of our method is illustrated in Figure 2. We facilitate the learning of adversarial the attacker by jointly solving two opposing tasks: (1) memorizing the underlying recognition cues for ReID of each identity via teacher-student memory mimicking. (2) interpolating this prior knowledge of VM to attacker to guide the efficient adversarial generation.

To avoid optimization collapse in solving such multiple opposing tasks, we deliberately separate two individual branches as much as possible and set the memory only writable and readable for mimicking and attack, respectively. In particular, the clean images x are sent to the mimicking branch composed by the subnet \mathcal{M}' of VM, memory module \mathcal{P} , to learn identity-wise structural prototypes. Afterward, the generator G of the attacker, composed of an encoder and a decoder, retrieves a similar but different identity prototype to generate, which determines to mislead the VM in prior. Meanwhile, according to the searchable realistic memory, the discriminator \mathcal{D} distinguishes the adversarial generation belonging to the identity it claimed, following the consistent identity preservation.

C. Teacher-student Memory Mimicking

Inspired by [1], we insert an external-attention memory module \mathcal{P} into VM to remember such prototypes in learnable tensor cache. Specifically, we keep and freeze the subnet \mathcal{M}' of VM before pooling, local split or equivalents to obtain spatial informative features where we can access the sampled-driven decision making process. Then, for following evaluation fairness, we apply the identical memory module \mathcal{P} , MaxPooling, Batch Normalization (BN) and classification head sequentially after \mathcal{M}' for different VMs. During fine-tuning for ReID, \mathcal{P} could dynamically record what VM recognizes images for each identity and what is real images embedded in latent space, *i.e.*, identity-wise structural prototype.

The prototype memory module \mathcal{P} contains N learnable identity prototypes which are recorded by a matrix $K \in \mathbf{R}^{N \times C}$ with fixed feature dimension C . Identity prototype number N is equal to the identity number of training set where each identity contains one prototype in memory. Then an attention-based addressing operator for accessing the memory, *i.e.*, memory reader and writer, is used to assign each image into spare prototypes. The role of memory reader and writer depends on whether K updates in current step. Given the output $\mathbf{f} \in \mathbf{R}^{H \times W \times C}$ of \mathcal{M}' in which H, W denote the height

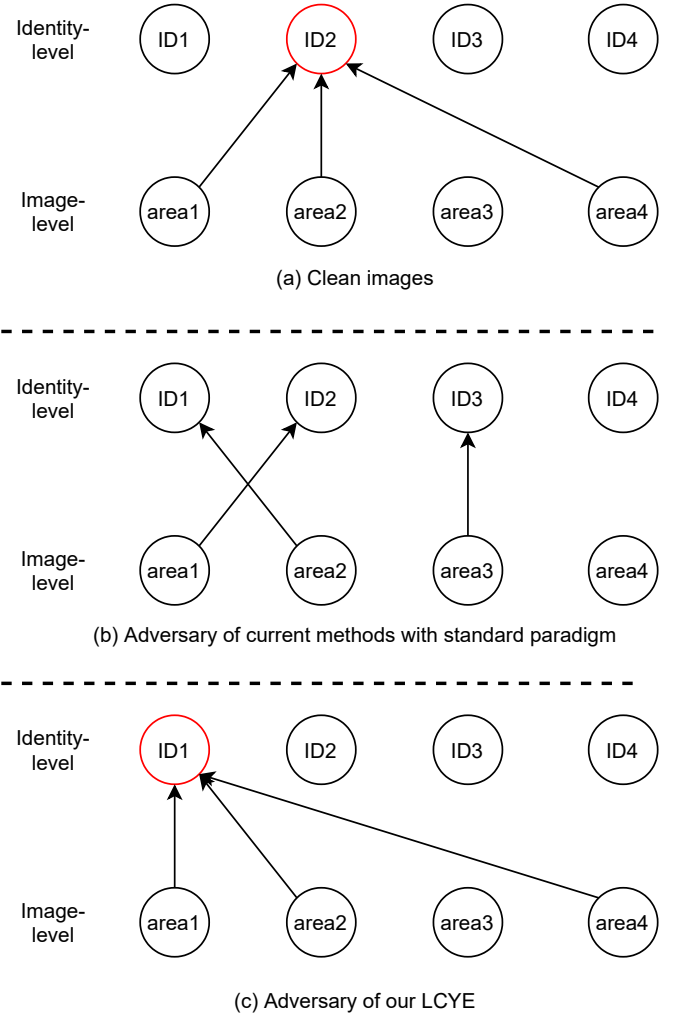


Fig. 3: Simple illustration of decision making of victim model using clean images, adversarial images generated by current methods and our LCYE. We omit the insignificant links from area to identity (ID).

and width resolution, our memory module could be denoted as:

$$w_{ij} = \frac{\exp(d(\mathbf{f}_i, \mathbf{k}_j))}{\sum_{j=1}^N \exp(d(\mathbf{f}_i, \mathbf{k}_j))} \quad (2)$$

where \mathbf{f}_i and \mathbf{k}_j are feature and prototype slice from input \mathbf{f} and prototype matrix K . w_{ij} is the normalized weight measuring the cosine similarity $d(\cdot, \cdot)$ between \mathbf{f}_i and \mathbf{k}_j . Thus, the assigned prototype $h \in \mathbf{R}^{H \times W \times C}$ from feature \mathbf{f} could be calculated as:

$$h = MRA(\mathbf{f}, K) = \sum_{i=1}^{H \times W} \sum_{j=1}^N w_{ij} \mathbf{k}_j \quad (3)$$

D. Memory-guided Adversarial Attacker

The motivation of our LCYE is to build a prototype-consistent generation for adversarial attack: The generator accords to one potential identity prototype to generate the

adversary, where the selected prototype claims the identity belonging to the adversary. Then the discriminator could also tell whether the adversary belong to the claimed identity via checking the prototype. Thus, our memory-guided attacker obtains three main components: adversarial generator \mathcal{G} to generate noise n , identity-wise multi-stage discriminator \mathcal{D} to ensure identity preservation consistency and a mask predictor \mathcal{O} to estimate the effective noise mask m . The final attack image is composed by $x' = m \cdot n + x$. Besides, VM's knowledge, learned and recorded in K , is interpolated into the generator and discriminator to facilitate the inconspicuous adversarial generation, meanwhile the mask predictor selects the location of recognition cues from VM for accurate hit. Given the real image x , our generator first encode it to f and let it retrieve target prototype from \mathcal{P} as attack cues h_{attack} to generate noise n :

$$n = \mathcal{G}(x, h_{attack}), h_{attack} = MRA(f, K) \quad (4)$$

Hence, mask predictor \mathcal{O} maps the location of discriminative region to image resolution as mask m according to the clues of spatial features \mathbf{f} from VM:

$$\mathbf{f} = \mathcal{M}'(x), m = \mathcal{O}(\mathbf{f}) \quad (5)$$

Finally, the multi-stage identity-aware discriminator classifies whether attack images x' and original images x meet the prototype belonging to the claimed identity. In particular, three subnetworks, receiving $\{1, 1/4, 1/16\}$ areas of the original images as the input, are introduced in \mathcal{D} to obtain multi-scale response. Then, by pyramiding the features of different levels of the discriminator as [9], a series of downsampled results with a ratio of $\{1/32, 1/16, 1/8, 1/4\}$ of the image are thus formulated for final prediction. We empirically let features $s_{1/4}$ with 1/4 resolution ratio to retrieve relevant prototype from K to check whether the image meets the imagination of VM. Solely interpolating VM knowledge to discriminator brings implicit external-internal semantic consistency but still lacks explicit identity consistency for personalized supervision. Therefore, \mathcal{D} is designed to estimate multi-identity probability $p \in \mathbf{R}^{N+1}$ where N is the total number of identities in training set and the additional dimension denotes the fake class.

$$p = \mathcal{D}(x, h_d), h_d = MRA(s_{1/4}, K) \quad (6)$$

Note this prototype interpolation in generator and discriminator seems to have no explicit map with one-hot ground truth, since the learnable prototype matrix K records the general representation of each identity but do not know the correspondence. It means LCYE lacks explicit and strict prototype supervision for each identity and we can only hope the model learns such the correspondence. However, this risk is mitigated by the adversarial generative mechanism and static memory reading. The competitive generator and discriminator can not lasso the memory module since they can only read it. In particular when the memory is meaningful for proxy recognition, the focus of competition thus moves to how to use the memory for better generation, rather than ignoring it.

E. Objective Function

The total objective includes (1) mis-ranking loss \mathcal{L}_{mr} for attack (2) GAN loss \mathcal{L}_{GAN} for personalized realistic generation (3) visual perception loss \mathcal{L}_{VP} for inconspicuous

change (4) cross-entropy loss \mathcal{L}_{ce} and triplet loss \mathcal{L}_{tri} for teacher-student mimicking:

$$\mathcal{L}_{attack} = \alpha_1 \cdot \mathcal{L}_{mr} + \alpha_2 \cdot \mathcal{L}_{GAN} + \alpha_3 \cdot \mathcal{L}_{VP} \quad (7)$$

$$\mathcal{L}_{mimic} = \beta_1 \cdot \mathcal{L}_{ce} + \beta_2 \cdot \mathcal{L}_{tri} \quad (8)$$

where α_* and β_* are tradeoff factors. \mathcal{L}_{attack} is the loss for attack branch while \mathcal{L}_{mimic} is for mimicking branch. Since the objectives are already proposed or largely identical as Mis-ranking [9] that we modify from, we prefer to discuss the capability of inserting VM's knowledge in attacker which eases the dependence on both mis-ranking loss \mathcal{L}_{mr} and visual perception loss \mathcal{L}_{VP} in Section IV-B. Empirically, we set $\alpha_1 = 1, \alpha_2 = 1, \alpha_3 = 1, \beta_1 = 1, \beta_2 = 1$. The detail of objectives is shown below.

The mis-ranking loss, i.e., attack loss, include four variants: (1) standard misclassification loss **cent**, (2) misclassification proposed by [9] **xent**, (3) adversarial triplet loss **etri**, (4) misclassification and adversarial triplet losses **xcent+etri**. We omit the description of standard misclassification loss **cent**, since it is a simple adversarial cross entropy loss. Given a clean image \mathcal{I} and its adversary $\hat{\mathcal{I}}$, the misclassification loss **xent** proposed by [9] is:

$$\mathcal{L}_{xent} = - \sum_{n=1}^N \mathcal{S}(\mathcal{T}(\hat{\mathcal{I}}))_n ((1 - \delta) \mathbf{H}_{argmin} \mathcal{T}(\mathcal{I})_n + \delta v_n) \quad (9)$$

where \mathcal{S} is the log-softmax function, N is the total identity number and $v = [\frac{1}{N-1}, \dots, 0, \dots, \frac{1}{N-1}]$ is smoothing regularization in which v_k equals to $\frac{1}{N-1}$ everywhere except when n is the ground-truth ID. \mathbf{H} is the indicator function. The adversarial triplet loss **etri** is:

$$\begin{aligned} \mathcal{L}_{etri} &= \sum_{n=1}^N \sum_{c=1}^{C_n} \left[\max_{\substack{j \neq n \\ j=1 \dots N \\ c_d=1 \dots C_j \\ \alpha_j}} \left\| \mathcal{T}(\hat{\mathcal{I}}_c^n) - \mathcal{T}(\hat{\mathcal{I}}_{c_d}^j) \right\|_2^2 \right] \\ &= - \min_{c_s=1 \dots C_n} \left[\left\| \mathcal{T}(\hat{\mathcal{I}}_c^n) - \mathcal{T}(\hat{\mathcal{I}}_{c_s}^n) \right\|_2^2 + \Delta \right]_+ \end{aligned} \quad (10)$$

where C_n is the number of samples drawn from the n -th person ID, \mathcal{I}_c^n is the c -th images of the n ID in a mini-batch, c_s and c_d are the samples from the same ID and the different IDs, $\|\cdot\|_2$ is the square of L2 norm used as the distance metric, and Δ is a margin threshold.

For visual perception loss, we borrow two choices of **SSIM** and **MS-SSIM** from [9]. The difference between them is interpolating multi-scale (**MS**) measurement. Therefore, we mainly represent **MS-SSIM** here:

$$\mathcal{L}_{MS-SSIM}(\mathcal{I}, \hat{\mathcal{I}}) = [l_L(\mathcal{I}, \hat{\mathcal{I}})]^{\alpha_L} \cdot \prod_{j=1}^L [c_j(\mathcal{I}, \hat{\mathcal{I}})]^{\beta_j} [s_j(\mathcal{I}, \hat{\mathcal{I}})]^{\gamma_j} \quad (11)$$

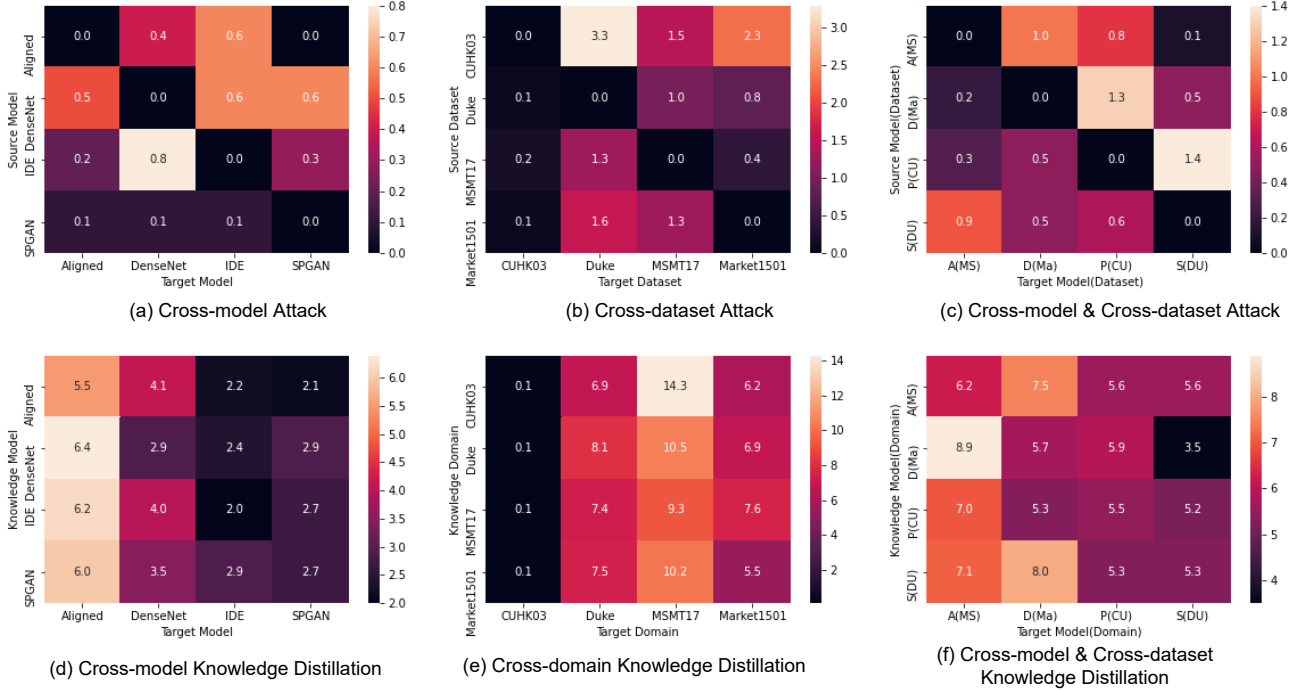


Fig. 4: Rank1 results (%) of *black-box attack* and cross-model/domain knowledge distillation. In cross-modal&dataset(domain) evaluation, we abbreviate AlignedReID(MSMT17)→A(MS), DenseNet(Market1501)→D(Ma), PCB(CUHK03)→P(CU), SPGAN(DukeMSMT)→S(DU).

TABLE I: Statistics of datasets used in the paper.

Dataset	Object	Identities	Images
Market1501	Person	1,501	32,688
CUHK03	Person	1,467	28,192
DukeMTMC	Person	1,404	34,183
MSMT17	Person	4,101	126,44

where c_j and s_j are the measures of the contrast comparison and the structure comparison at the j -th scale respectively, which are calculated by $c_j(\mathcal{I}, \hat{\mathcal{I}}) = \frac{2\sigma_{\mathcal{I}\hat{\mathcal{I}}} + C_2}{\sigma_{\mathcal{I}}^2 + \sigma_{\hat{\mathcal{I}}}^2 + C_2}$ and $s_j(\mathcal{I}, \hat{\mathcal{I}}) = \frac{\sigma_{\mathcal{I}\hat{\mathcal{I}}} + C_3}{\sigma_{\mathcal{I}}\sigma_{\hat{\mathcal{I}}} + C_3}$ where σ is the variance/covariance.

For GAN loss, we adopt the multi-discriminator and multi-label GAN loss as:

$$\mathcal{L}_{GAN} = \mathbf{E}_{(I_{cd}, I_{cs})} [\log \mathcal{D}_{1,2,3}(I_{cd}, I_{cs})] + \mathbf{E}_{\mathcal{I}} \left[\log \left(1 - \mathcal{D}_{1,2,3}(\mathcal{I}, \hat{\mathcal{I}}) \right) \right] \quad (12)$$

where the subscript 1, 2, 3 denote our multi-stage discriminator. The identity-aware supervision could be deemed as the multi-label binary version of standard real/fake loss.

F. How Memory Help Attack?

Intuitively, prototype memory module records the recognition knowledge of victim model and further help attack process. But does it really work and how? We first remove the mis-ranking loss \mathcal{L}_{mr} and find the attack performance only drops slightly (see two rows in Figure 4). It means the recognition knowledge does facilitate adversarial attack.

Moreover, to answer how it works, we should first reflect the problem setup in Sec. III-A. (1) The pixel-level adversarial guidance is provided by mask predictor and memory reading

of generator. These two modules estimate where to attack in spatial resolution and which identity to become in latent feature. Compared to previous methods [9], they either lack controllable manipulation or provide adversarial supervision via misclassification loss. (2) For characteristic design of victim model, our LCYE solves this issue by the universal teacher-student mimicking. Different from find the adversarial counterpart of their design, *i.e.*, hard adversarial triplet loss and hard triplet loss, LCYE keeps all the structures and schemes of victim model and leverages a multiple opposing task framework. (3) The prototype interpolation and identity aware generation, referred as category cycle consistency, ensure each changed region is for the recognition of target identity. As shown in Figure 3, standard paradigm scatters the contribution of areas to different identities. While our method redirects the map from each salient locality to the same wrong higher semantics since it assigns the same identity prototype to the image.

IV. EXPERIMENTS

Datasets: Four ReID benchmarks are used for the evaluation of our method, including Market1501 [14], CUHK03 [53], DukeMTMC [15] and MSMT17 [54].

For attack evaluation metrics, we use Rank{1, 5, 10} and mAP for ReID attack where the lower numerical value means better success attack rate in an attack problem. The details of these datasets are summarized in Table I.

Market1501 consists of 32,688 images of pedestrians taken by six cameras. There are 1,501 different persons in this dataset. For each person, there are 3.6 images on average under

TABLE II: Attacking the state-of-the-art ReID systems on Market1501, CUHK03, and DukeMTMC. **blue** and **red** denote previous best and current best results. \downarrow means the lower numerical value is better for attack.

Methods with Market1501		Rank1 \downarrow				Rank5 \downarrow				Rank10 \downarrow				mAP \downarrow			
		Before	PGD	MR	Ours	Before	PGD	MR	Ours	Before	PGD	MR	Ours	Before	PGD	MR	Ours
Backbone	IDE(ResNet50)	83.1	4.5	3.7	0.3	91.7	8.7	8.3	1.2	94.6	12.1	11.5	2.4	63.3	4.6	4.4	0.3
	DenseNet121	89.9	1.2	1.2	0	96.0	1.0	1.3	0.2	97.3	1.5	2.1	0.4	73.7	1.3	1.3	0.2
	Mudeep(Inceptionv3)	73.0	2.6	1.7	0.0	90.1	5.5	1.7	0.2	93.1	6.9	5.0	0.5	49.9	2.0	1.8	0.2
	AlignedReID	91.8	10.2	1.4	0.1	97.0	15.8	3.7	0.9	98.1	19.1	5.4	1.8	79.1	8.9	2.3	0.3
Part-Aligned	PCB	88.6	6.1	5.0	0.0	95.5	12.7	10.7	0.1	97.3	15.8	14.3	0.2	70.7	4.8	4.3	0.2
	HACNN	90.6	6.1	0.9	2.8	95.9	8.8	1.4	8.1	97.4	10.6	2.3	12.9	75.3	5.3	1.5	1.2
	CamStyle+Era(IDE)	86.6	15.4	3.9	0.1	95.0	23.9	7.5	0.7	96.6	29.1	10.0	1.4	70.8	12.6	4.2	0.2
GAN	LSRO(DenseNet121)	89.9	7.2	0.9	0.8	96.1	13.1	2.2	2.2	97.4	15.2	3.1	3.5	77.2	8.1	1.3	1.7
	HHL(IDE)	82.3	5.7	3.6	0.1	92.6	9.8	7.3	0.7	95.4	12.2	9.7	1.4	64.3	5.5	4.1	0.2
	SPGAN(IDE)	84.3	10.1	1.5	0.0	94.1	16.7	3.1	0.6	96.4	20.9	4.3	1.6	66.6	8.6	1.6	0.2
	TransReID(ViT+baseline)	94.6	-	6.2	0.9	98.2	-	10.0	1.5	99.2	-	12.1	2.7	87.1	-	6.3	0.8
Transformer	TransReID(ViT)	95.1	-	5.2	0.9	98.4	-	10.1	1.7	99.1	-	12.0	2.6	89.0	-	6.5	0.9

Methods with CUHK03		Rank1 \downarrow				Rank5 \downarrow				Rank10 \downarrow				mAP \downarrow			
		Before	PGD	MS	Ours	Before	PGD	MS	Ours	Before	PGD	MS	Ours	Before	PGD	MS	Ours
Backbone	IDE(ResNet50)	24.9	0.8	0.4	0.0	43.3	1.2	0.7	0.4	51.8	2.1	1.5	0.4	24.5	0.8	0.9	0.2
	DenseNet121	48.4	0.1	0.0	0.0	50.1	0.1	0.2	0.6	70.1	0.3	0.6	1.2	84.0	0.2	0.3	0.4
	Mudeep(Inceptionv3)	32.1	0.4	0.1	0.0	53.3	1.0	0.5	0.2	64.1	1.5	0.8	0.4	30.1	0.8	0.3	0.1
	AlignedReID	61.5	1.4	1.4	0.0	79.4	2.2	3.7	0.6	85.5	4.1	5.4	1.1	59.6	2.1	2.1	0.3
Part-Aligned	PCB	50.6	0.5	0.2	0.0	71.4	2.1	1.3	0.2	78.7	4.5	1.8	0.8	48.6	1.2	0.8	0.3
	HACNN	48.0	0.4	0.1	0.0	69.0	0.9	0.3	0.4	78.1	1.3	0.4	1.1	47.6	0.8	0.4	0.3

Methods with DukeMTMC		Rank1 \downarrow				Rank5 \downarrow				Rank10 \downarrow				mAP \downarrow			
		Before	PGD	MR	Ours	Before	PGD	MR	Ours	Before	PGD	MR	Ours	Before	PGD	MR	Ours
GAN-based	CamStyle+Era(IDE)	76.5	22.9	1.2	0.6	86.8	34.1	2.6	1.5	90.0	39.9	3.4	2.6	58.1	16.8	1.5	0.3
	LSRO(DenseNet121)	72.0	7.2	0.7	0.5	85.7	12.5	1.6	1.4	89.5	18.4	2.2	2.2	55.2	8.1	0.9	0.8
	HHL(IDE)	71.4	9.5	1.0	0.1	83.5	15.6	2.0	0.8	87.7	19.0	2.5	1.7	51.8	7.4	1.3	0.2
	SPGAN(IDE)	73.6	12.4	0.1	0.4	85.2	21.1	0.5	1.2	88.9	26.3	0.6	2.5	54.6	10.2	0.3	0.3
	TransReID																

each camera. These images can be classified into two types, which are images detected buy the DPM automatically and cropped images.

CUHK03 consists of 28,192 images of 1,467 persons which were taken by two campus cameras. Each person appears in two views. Manually labelled bounding boxes and detected bounding boxes are two types of annotations in this dataset. Besides, 20 test sets which each contains 100 identities are provided.

DukeMTMC is made up of 34,183 bounding boxes of 1,404 pedestrians. These images were taken by eight cameras. For training set, it has 16,522 bounding boxes of 702 persons. The other pedestrians are for test set.

MSMT17 is an image based person ReID dataset. It has 126,44 images of 4,101 identities. The dataset is captured by 15 cameras. The training set has 93,820 bounding boxes of 3,060 persons.

Implementation Details: We use batch size 32, learning rate 0.0002 for GAN and 0.0003 for mimicking on a single GTX P40 GPU. We use **xent+etri** for misranking loss \mathcal{L}_{mr} and **MS-SSIM** for visual perception loss \mathcal{L}_{VP} . The triplet margin is set to 0.3 for mimicking and attack branches. In comparison with other attackers, we use full size image as possible mask to attack. Our generator uses ResNet Block with $4\times$ downsampling and $4\times$ upsampling. The sub-discriminator adopts the basic structure from Mis-ranking. For target attack, since ReID is an open-set task where training and test sets have non-overlapping identities, it is unfeasible to follow close-set target attack. We separate it as two evaluation: target consistency on adversarial query images and standard attack. For each identity $n \in N$, we randomly select γ query images for each identity to generate adversarial query images with total number $\gamma \cdot N$. Then we sent these images to victim model and calculate the Euclidean distance of their embeddings. With pseudo labels, we calculate the Rank1 accuracy as their target consistency.

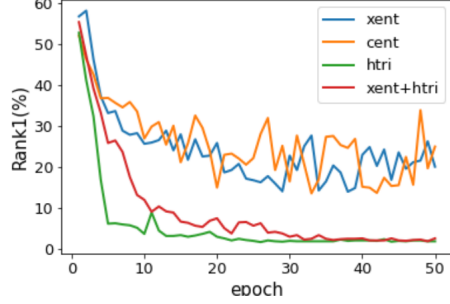
TABLE III: Target attack results (%) on Market1501.

Method	Target Consistency		Attack	
	Rank1 \uparrow	Rank1 \downarrow	mAP \downarrow	
DenseNet121	71.2	2.0	1.3	
AlignedReID	78.6	4.2	1.7	
SPGAN	63.6	1.2	1.4	
TransReID	45.0	2.1	2.0	

Implementation Details and Protocols: Our victim models include CNN-based methods (AlignedReID [55], DenseNet [17], etc [56]–[58]), GAN-based methods (CamStyle [59], SPGAN [60], LSRO[61], HHL[62]) and Transformer-based methods (TransReID [2]). The basic framework of our LCYE is largely benefited from Mis-ranking [9], including the hyper-parameters, basic model structure etc, therefore, we compare with it in ablation to verify the capability brought from VM knowledge. For fair comparison, we adopt the same protocols as [9] by L_∞ -bounded attacks with $\varepsilon = 16$. The *black-box attack* includes cross-model attack, cross-dataset attack and cross-model-dataset attack as the standard setting. For the *target attack*, we achieve it by modifying Equation 3 to $\sum_{i=1}^{H \times W} \sum_{j=1}^N w_{ij} \mathbf{q}_i \mathbf{k}_j$ where $\mathbf{q}_i \in Q \in \mathbf{R}^{N \times 1}$ is the indicator of selected identity and adding corresponding identity consistency supervision in GAN. Due to the open-set essence of ReID task, we evaluate the target attack performance by (1) the similarity matrix of embeddings of adversarial query images which is simplified as Rank1 \uparrow as target consistency, (2) the attack success rate, i.e., Rank1 \downarrow and mAP \downarrow .

For the ablation study, we clarify that (1) *baseline mimicking* is to let \mathcal{M}' fixed and learn the memory, (2) *online mimicking* is to allow \mathcal{M}' pretrained on ImageNet to update with mimicking branch (learn from scratch as a ReID task) and (3) *offline mimicking* is to first train mimicking branch with fixed \mathcal{M}' and then train the pending attack branch. If without specific instruction, all ablation experiments is done on AlignedReID with Market1501.

(a) Mis-ranking with different attack losses



(b) Our LCYE with different attack losses

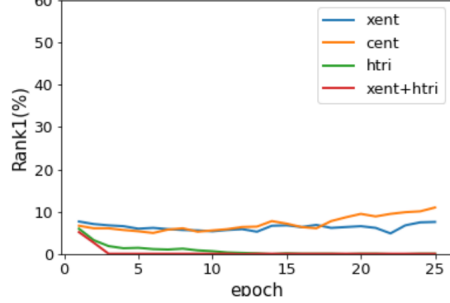


Fig. 5: Ablation on sensitivity of different losses. (a) and (b) record the test evaluation results after each epoch.

A. Attacking State-of-the-Art ReID Models

White-box Attack In Table II, we demonstrate the superior performance of our method to other attackers. Results on multiple datasets and models show that our LCYE largely improves the attack success scope within 1% for Rank1, 3% for Rank5, 4% for Rank10 and 2% for mAP respectively in most cases. Moreover, our method performs favorably against Mis-ranking (MR) and PGD [63] with a large margin on different lines of ReID models.

Black-box Attack Figure 4 shows the cross-model & cross-dataset & cross-model-dataset evaluation. Benefiting from cheating VM’s knowledge, our method achieves similar attack performance as white-box attack. We find that training on domain adaption SPGAN seems to be more versatile than others in cross model case, and results on CUHK03 in cross dataset evaluation show the domain-specific vulnerability.

Target Attack To the best of our knowledge, our LCYE is the first method of target attack on ReID. In Table III, our method could successfully transfer the prototype of desired identity to arbitrary images with over 60% consistency accuracy and high attack performance, except on TransReID. One possible reason is that comparing to CNN, Transformers always focus on larger area of recognition cues that makes personalized target attack harder. Moreover, comparing to *non-target attack*, i.e., white-box attack, the performance only drops 2%, 4.1%, 1.2% and 1.2% for four models respectively. It indicates our LCYE is not sensitive to the personalized assignment.

TABLE IV: Results (%) of using different knowledge model \mathcal{M}' to attack target model \mathcal{M} with attack loss on Market1501.

\mathcal{M}	\mathcal{M}'	R1	R5	R10	R20	mAP
DenseNet	IDE	0.0	0.0	0.0	0.3	0.1
DenseNet	AlignedReID	0.0	0.3	0.9	2.3	0.2
DenseNet	SPGAN	0.1	0.5	1.0	2.2	0.2
AlignedReID	IDE	0.6	2.1	3.6	5.8	0.4
AlignedReID	DenseNet	0.4	1.0	1.9	3.8	0.3
AlignedReID	SPGAN	0.0	0.4	0.9	1.9	0.2
IDE	AlignedReID	0.1	0.5	1.1	2.0	0.2
IDE	DenseNet	0.2	0.7	1.4	2.4	0.2
IDE	SPGAN	0.2	1.5	2.5	4.6	0.3

TABLE V: Ablation on ‘does the memory learn the belief of victim model?’ with three mimicking variants. ReID results is evaluated on mimicking branch.

Mimicking	ReID		Attack	
	Rank1 \uparrow	mAP \uparrow	Rank1 \downarrow	mAP \downarrow
baseline	61.3	54.2	5.5	2.1
online	85.2	74.3	5.6	2.1
offline	61.3	54.2	5.5	2.1

B. Ablation Study

Cross-model & Cross-domain Knowledge Distillation

For cross-domain adaption and cross-model consensus, we simply use different \mathcal{M}' to attack \mathcal{M} and find their attack performance is unexpectedly good without obvious distinction with Table II. We believe the strong attack supervision may direct the whole optimization to an aggressive way. Thus, we choose to remove the misranking loss \mathcal{L}_{mr} to check the model consensus for better interpretability. Note this experiment is similar to black-box attack in meaning but free from attack guidance. As shown in Figure 4 (d)-(e), the diversity of knowledge consensus from models is larger than from domains. Expect CUHK03 which also achieves lowest value in cross-dataset attack, the result of all domain seems to be uniform. This find is also consistent with cross-model-dataset, indicating domain distribution makes less senses than model structure for knowledge commonsense of robustness.

In this experiment, we provide the results of using different \mathcal{M}' to attack \mathcal{M} with **attack loss**. As shown in Table IV, our LCYE achieves a similar performance as Table 1 in original paper. For cross-domain knowledge distillation, it shows a similar good performance. Thus, we believe the attack supervision may lead the whole optimization to an aggressive without showing the knowledge property of target model \mathcal{M} and knowledge model \mathcal{M}' .

Online Mimicking and Offline Mimicking One common concern is that *does the memory really learn the belief of victim model?* One explanation is cross model/domain knowledge distillation and *target attack* which show the distinct knowledge of each model and possibility for attack. Besides, to figure out the influence of mimicking manner in the interaction with attacker, we make experiments with three variants, i.e., *baseline mimicking*, *online mimicking*, *offline mimicking*, without attack loss. As shown in Table V, ReID results evaluate the leftover property of mimicking branch after our simple mimicking manner. The identical results of *baseline* and *offline* means the memory module is not affected by attack branch during training and the quality of memory doesn’t influence the performance of attacker (joint training

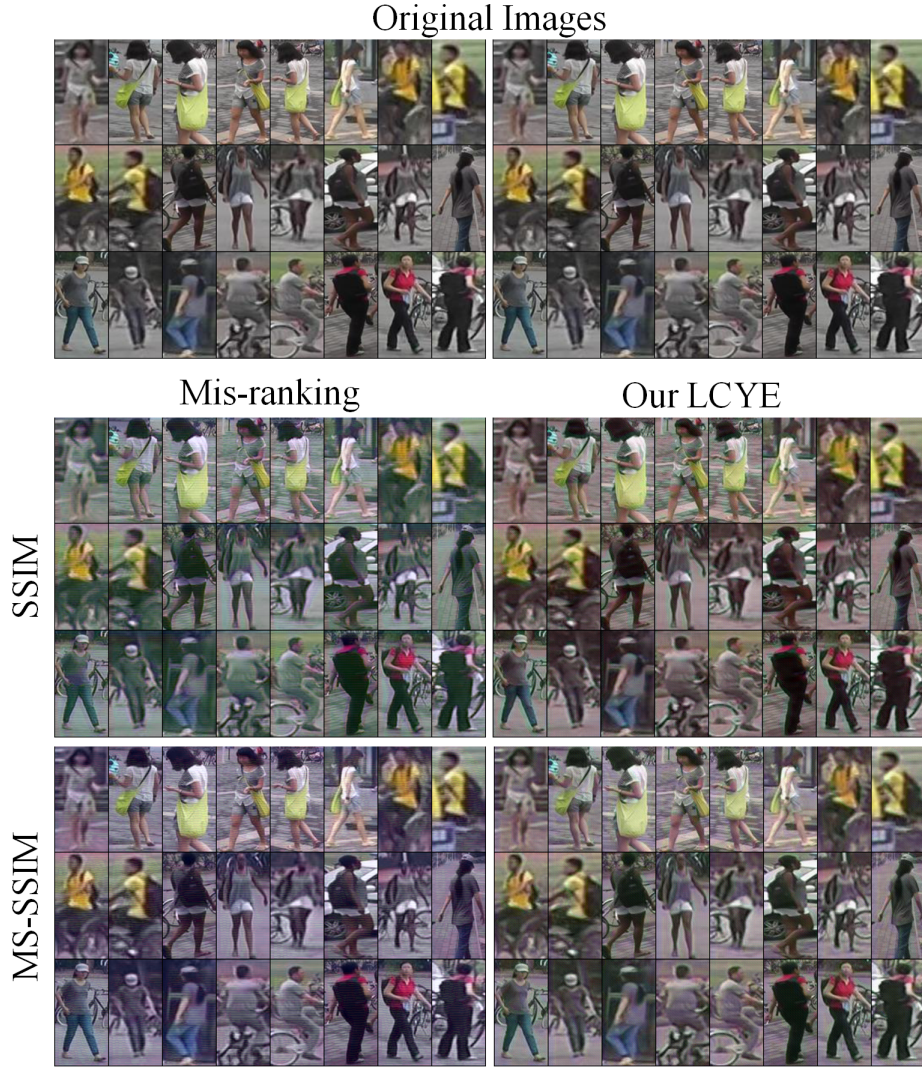


Fig. 6: Visualization of using different visual perception losses for Mis-ranking and our method.

TABLE VI: Proportion of adversarial points. † denotes the results with appropriate relaxation. The ratio denotes the adversarial points/total points.

Ratio	Mis-ranking		ours	
	Rank1	mAP	Rank1	mAP
full size	1.4	2.3	0.1	0.3
1/2	39.3	31.5	11.1	3.6
1/4	72.7	85.9	11.1	3.5
1/8	91.8	79.1	11.1	3.5
1/16	91.8	79.1	11.0	3.5
1/16†	8.2	14.7	1.3	0.6
1/32†	59.4	47.3	1.3	0.7
1/64 †	75.5	61.5	1.6	1.0

and two-stage training is different from memory retrieved by attacker in each iteration). Furthermore, the obtained memory of *online* is different from that of victim model since the model structure is partly different. But the performance doesn't drop for this knowledge difference. We owe this phenomenon to the effectiveness of our LCYE paradigm which is not sensitive to the knowledge.

Sensitivity of Different Losses Mis-ranking heavily relies on attack loss $\mathcal{L}_{mr} \in \{\text{cent}, \text{xent}, \text{etri}, \text{xcent+etri}\}$ and $\mathcal{L}_{VP} \in \{\text{SSIM}, \text{MS-SSIM}\}$, since it needs enough adversarial feedback via overturing victim model. In Figure 5 (a) and (b), our LCYE has sharper and more stable curves than Mis-ranking using different attack losses, indicating the memory reduces the necessity of well-designed objectives. This observation is also consistent with Figure 4 (d)-(f) where without attack supervision our LCYE also achieves promising attack performance. Moreover, we also ablate the dependence on visual perception loss. As shown in Figure 6, our method has a more inconspicuous visualization than the counterpart without dark purple or green background. Thus, exquisite losses isn't the necessity of our LCYE.

Sensitivity of Visual Perception Loss: As shown in Figure 6, we provide more visualization to analyze insensitivity of our method to different objectives. We can find that our method poses less dark green or purple background on original images and generates clearer images without heavy blur. We contribute this benefit to the interpolation of VM knowledge

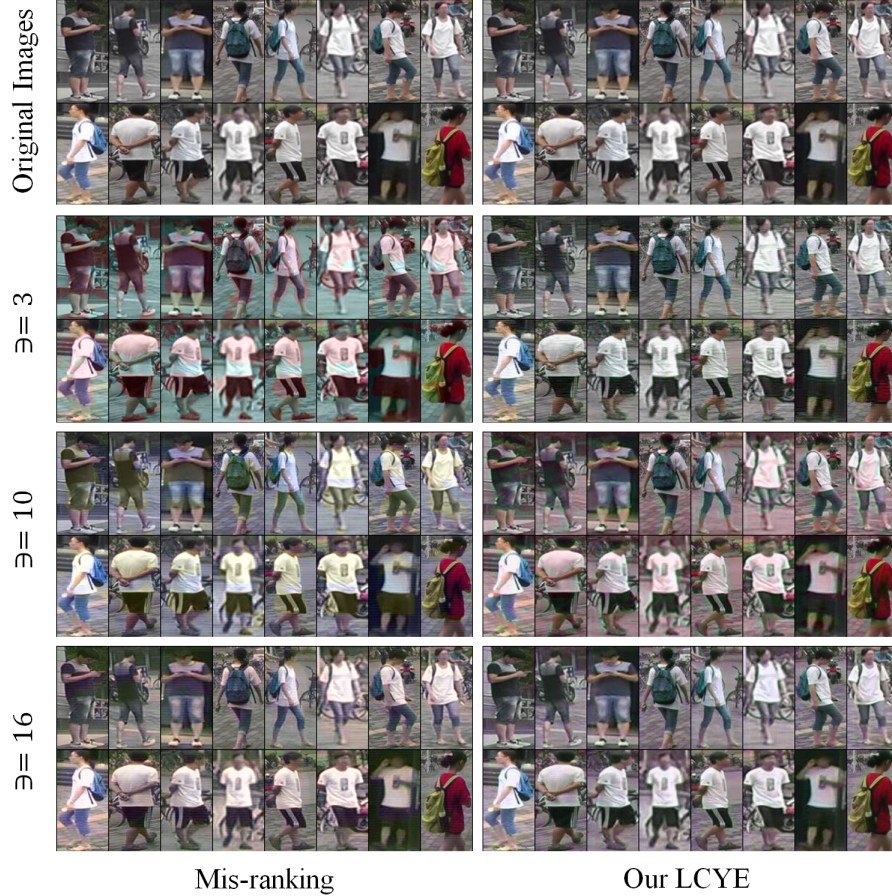


Fig. 7: Visualization of using different visual perception losses for Mis-ranking and our method.

TABLE VII: Ablation on different ε . The results is reported on AlignedReID with Market1501.

	Mis-ranking				ours			
	R1	R5	R10	mAP	R1	R5	R10	mAP
40	0.0	0.2	0.6	0.2	0.0	0.1	0.1	0.0
20	0.1	0.4	0.8	0.4	0.0	0.1	0.1	0.0
16	1.4	3.7	5.4	2.3	0.1	0.9	1.8	0.3
10	24.4	38.5	46.6	21.0	0.4	1.6	3.2	0.3
5	69.2	82.6	87.0	56.4	4.2	10.2	15.1	1.6
3	83.9	92.5	95.1	70.2	8.1	18.1	23.8	2.7

to both generator and discriminator, since it also conveys the configuration of realistic images.

Number of the Pixels to be Attacked We further ablate the pixel demand of our method to attack in Table VI. Our LCYE achieves promising performance even with small ratio. Note that it keeps 11.1% Rank1 and 3.6% mAP from 1/2 to 1/16, we believe LCYE needs much fewer pixels than other attacker. The relaxation only brings about less than 10% improvement, comparing to Mis-ranking that heavily depends on it. This benefit may come from the accurate hit of our mask predictor which points out the salient region believed by victim model.

Comparisons of Different ε Larger ε could effectively boost attack performance but sacrifice the visual quality. We

manually control the magnitude of ε to verify the effectiveness of our LCYE. As shown in Table VII, smaller ε would not limit our attack performance. It meets the lower bound (0.4%) of Rank1 at $\varepsilon = 10$ or even much early. Especially when using $\varepsilon = 10$ or 5, our LCYE also shows promising superiority over Mis-ranking with 20%-60% gains. We further provide visualization comparison in Figure 7. With small magnitudes of ε , Mis-ranking not only has strong blue atmospheres and obvious color blocks over original images, but also poses striped Gaussian blur. But for our method, it generates much more reasonable adversary comparing to Mis-ranking.

Cycle Consistency for Generation Our LCYE keeps cycle consistency via identity-aware adversarial learning and interpolating VM knowledge to generator and discriminator, which are termed as explicit and implicit guidance. Figure 8 shows the noise and adversary visualization where the cycle consistency facilitates the inconspicuous perception. From the mask graphs on the right, Our model captures human silhouettes clearly.

Discussion The transferability of ReID models is always evaluated by applying it on another dataset where the uninspiring results usually show the poor generalization ability of models. We instead analyze the commonsense of vulnerability of different models/domains and find that even without attack guidance, the domain-specific and model-specific decision making is fragile with minor distribution shift coming from

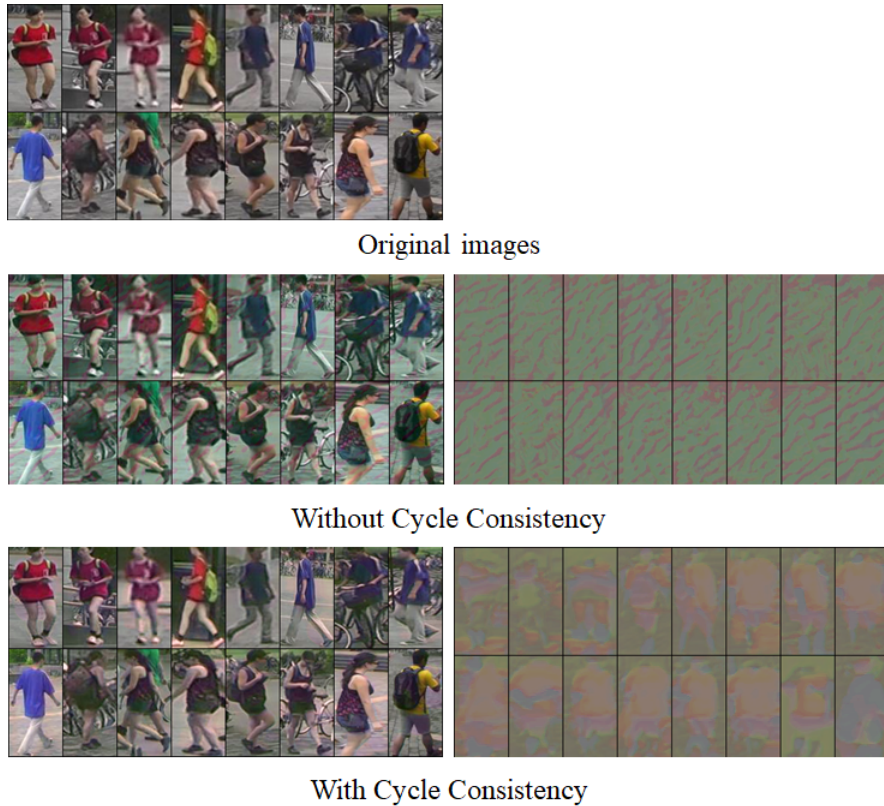


Fig. 8: Visualization of our LCYE with/without cycle consistent ency.

the knowledge belonging to others or even themselves. It means the improvement brought from either data augmentation (GAN) or local-awareness (Transformer) can not facilitate the robustness across models and domains in robustness.

We reconsider the capability of our LCYE, including lower pixel demand and lower objective dependency, from the aspect of inverse reinforcement learning. Namely, the attacker estimates a possible distribution of adversary by the attack award from victim models. Our LCYE is benefit from (1) a more direct way to observe and memorize the environment (VM) (2) providing dense awards for each pixel. In particular, the memory module is a shortcut interface accessing the decision making process of victim model, rather than indirectly predicting it by attack award. As shown in Figure 3, we simply illustrate the decision making from image-level to identity-level in neurons. Our method redirects the map from each salient locality to the same wrong higher semantics since it assigns the same identity prototype to the image while current methods always scatter them without pixel-level supervision.

Complexity Comparison As shown in Table VIII, our LCYE could boost the performance in a large margin with minor complexity addition. The additional parameter complexity mainly comes from the prototype memory module in both training and testing. Besides, The FLOPs complexity is largely increased in training since victim model needs to process clean image for mimicking branch, while in testing, we directly use the memory module for attack without processing images in victim model again.

TABLE VIII: Complexity comparison with baseline model in training and testing.

Model	Traning		Testing	
	baseline	LCYE	baseline	LCYE
Paras	2.5616×10^7	3.0021×10^7	1.9508×10^7	2.4733×10^7
FLOPs	1.9899×10^9	3.6822×10^9	1.3614×10^9	2.8385×10^9

V. CONCLUSION AND FUTURE WORK

In this paper, we propose our LCYE to attack victim models by cheating their mind. Different from current attackers using standard attack paradigm, our LCYE boosts the accessibility of the decision making process of victim models by our teacher-student mimicking. We also make extensive experiments on the knowledge commonsense of vulnerability across domains and models. Our LCYE is a transferable attacker with promising performance on white-box, black-box and target attack.

We tackle the robustness attack and generalization attack jointly without further refined manipulation. However, currently, generalization capability like domain adaptation and domain generalization, are independently discussed which is inversely represented as out-of-distribution non-transferable attack in this case. For example, AlignedReID trained on Market1501 could also achieve promising results on CUHK03 and DukeMTMC. Out-of-distribution non-transferable attack could specifically influence its performance on CUHK03 while never hurt it on Market1501 and DukeMTMC. This conditional and directional attack is much dangerous than the standard one

and could further connect model interpretability from positive (proxy tasks like classification and retrieve) and negative (adversarial attack) aspects. We believe future work could focus on this topic, with the help of explicit victim model knowledge.

REFERENCES

- [1] F. Chen, F. Wu, Q. Wu, and Z. Wan, “Memory regulation and alignment toward generalizer rgb-infrared person re-identification,” *arXiv preprint arXiv:2109.08843*, 2021.
- [2] S. He, H. Luo, P. Wang, F. Wang, H. Li, and W. Jiang, “Transreid: Transformer-based object re-identification,” *arXiv preprint arXiv:2102.04378*, 2021.
- [3] J. Li, S. Zhang, Q. Tian, M. Wang, and W. Gao, “Pose-guided representation learning for person re-identification,” *IEEE transactions on pattern analysis and machine intelligence*, 2019.
- [4] D. Li, X. Wei, X. Hong, and Y. Gong, “Infrared-visible cross-modal person re-identification with an x modality,” in *AAAI*, vol. 34, 2020, pp. 4610–4617.
- [5] X. Wei, D. Li, X. Hong, W. Ke, and Y. Gong, “Co-attentive lifting for infrared-visible person re-identification,” in *Proceedings of the 28th ACM International Conference on Multimedia*, 2020, pp. 1028–1037.
- [6] D. Cheng, Y. Gong, S. Zhou, J. Wang, and N. Zheng, “Person re-identification by multi-channel parts-based cnn with improved triplet loss function,” in *CVPR*, 2016, pp. 1335–1344.
- [7] L. Wei, S. Zhang, H. Yao, W. Gao, and Q. Tian, “Glad: Global-local-alignment descriptor for scalable person re-identification,” *IEEE Transactions on Multimedia*, vol. 21, no. 4, pp. 986–999, 2018.
- [8] J. Li, S. Zhang, and T. Huang, “Multi-scale 3d convolution network for video based person re-identification,” in *AAAI*, vol. 33, 2019, pp. 8618–8625.
- [9] H. Wang, G. Wang, Y. Li, D. Zhang, and L. Lin, “Transferable, controllable, and inconspicuous adversarial attacks on person re-identification with deep mis-ranking,” in *CVPR*, 2020, pp. 342–351.
- [10] S. Bai, Y. Li, Y. Zhou, Q. Li, and P. H. Torr, “Metric attack and defense for person re-identification,” *arXiv e-prints*, arXiv:1901, 2019.
- [11] Y. Sun, L. Zheng, Y. Yang, Q. Tian, and S. Wang, “Beyond part models: Person retrieval with refined part pooling (and a strong convolutional baseline),” in *ECCV*, 2018, pp. 480–496.
- [12] Y. Sun, C. Cheng, Y. Zhang, C. Zhang, L. Zheng, Z. Wang, and Y. Wei, “Circle loss: A unified perspective of pair similarity optimization,” in *CVPR*, 2020, pp. 6398–6407.
- [13] D. Wang and S. Zhang, “Unsupervised person re-identification via multi-label classification,” in *CVPR*, 2020, pp. 10 981–10 990.
- [14] L. Zheng, L. Shen, L. Tian, S. Wang, J. Wang, and Q. Tian, “Scalable person re-identification: A benchmark,” in *ICCV*, 2015, pp. 1116–1124.
- [15] E. Ristani, F. Solera, R. Zou, R. Cucchiara, and C. Tomasi, “Performance measures and a data set for multi-target, multi-camera tracking,” in *ECCV*, Springer, 2016, pp. 17–35.
- [16] S. Liao and L. Shao, “Interpretable and generalizable person re-identification with query-adaptive convolution and temporal lifting,” in *ECCV*, 2020, pp. 456–474.
- [17] G. Huang, Z. Liu, L. Van Der Maaten, and K. Q. Weinberger, “Densely connected convolutional networks,” in *CVPR*, 2017, pp. 4700–4708.
- [18] Y. Dong, F. Liao, T. Pang, H. Su, J. Zhu, X. Hu, and J. Li, “Boosting adversarial attacks with momentum,” in *Proceedings of the IEEE conference on computer vision and pattern recognition*, 2018, pp. 9185–9193.
- [19] F. Tramèr, N. Papernot, I. Goodfellow, D. Boneh, and P. McDaniel, “The space of transferable adversarial examples,” *arXiv preprint arXiv:1704.03453*, 2017.
- [20] W. Zhou, X. Hou, Y. Chen, M. Tang, X. Huang, X. Gan, and Y. Yang, “Transferable adversarial perturbations,” in *Proceedings of the European Conference on Computer Vision (ECCV)*, 2018, pp. 452–467.
- [21] Z. Zhong, L. Zheng, D. Cao, and S. Li, “Re-ranking person re-identification with k-reciprocal encoding,” in *CVPR*, 2017, pp. 1318–1327.
- [22] G. Chen, Y. Lu, J. Lu, and J. Zhou, “Deep credible metric learning for unsupervised domain adaptation person re-identification,” in *ECCV*, Springer, 2020, pp. 643–659.
- [23] J. Wang, Z. Wang, C. Liang, C. Gao, and N. Sang, “Equidistance constrained metric learning for person re-identification,” *Pattern Recognition*, vol. 74, pp. 38–51, 2018.
- [24] S.E.Fahlman and C.Lebiere, “The cascade-correlation learning architecture,” in *NIPS*, 1989, pp. 524–532.
- [25] B. M. Wilamowski and H. Yu, “Neural network learning without backpropagation,” *IEEE Transactions on Neural Networks*, vol. 21, no. 11, pp. 1793–1803, 2010.
- [26] B. Hariharan, P. Arbeláez, R. Girshick, and J. Malik, “Hypercolumns for object segmentation and fine-grained localization,” in *Proceedings of the IEEE conference on computer vision and pattern recognition*, 2015, pp. 447–456.
- [27] J. Long, E. Shelhamer, and T. Darrell, “Fully convolutional networks for semantic segmentation,” in *Proceedings of the IEEE conference on computer vision and pattern recognition*, 2015, pp. 3431–3440.
- [28] P. Sermanet, K. Kavukcuoglu, S. Chintala, and Y. LeCun, “Pedestrian detection with unsupervised multi-stage feature learning,” in *Proceedings of the IEEE conference on computer vision and pattern recognition*, 2013, pp. 3626–3633.
- [29] S. Yang and D. Ramanan, “Multi-scale recognition with dag-cnns,” in *Proceedings of the IEEE international conference on computer vision*, 2015, pp. 1215–1223.
- [30] C. Cortes, X. Gonzalvo, V. Kuznetsov, M. Mohri, and S. Yang, “Adanet: Adaptive structural learning of artificial neural networks,” in *International conference on machine learning*, PMLR, 2017, pp. 874–883.
- [31] R. K. Srivastava, K. Greff, and J. Schmidhuber, “Training very deep networks,” *Advances in neural information processing systems*, vol. 28, 2015.
- [32] K. He, X. Zhang, S. Ren, and J. Sun, “Deep residual learning for image recognition,” in *CVPR*, 2016, pp. 770–778.

- [33] —, “Identity mappings in deep residual networks,” in *European conference on computer vision*, Springer, 2016, pp. 630–645.
- [34] B. Harwood, V. Kumar BG, G. Carneiro, I. Reid, and T. Drummond, “Smart mining for deep metric learning,” in *Proceedings of the IEEE International Conference on Computer Vision*, 2017, pp. 2821–2829.
- [35] A. Hermans, L. Beyer, and B. Leibe, “In defense of the triplet loss for person re-identification,” *arXiv preprint arXiv:1703.07737*, 2017.
- [36] A. Dosovitskiy, L. Beyer, A. Kolesnikov, D. Weissenborn, X. Zhai, T. Unterthiner, M. Dehghani, M. Minderer, G. Heigold, S. Gelly, *et al.*, “An image is worth 16x16 words: Transformers for image recognition at scale,” *arXiv preprint arXiv:2010.11929*, 2020.
- [37] X. Jin, C. Lan, W. Zeng, Z. Chen, and L. Zhang, “Style normalization and restitution for generalizable person re-identification,” in *proceedings of the IEEE/CVF conference on computer vision and pattern recognition*, 2020, pp. 3143–3152.
- [38] J. Song, Y. Yang, Y.-Z. Song, T. Xiang, and T. M. Hospedales, “Generalizable person re-identification by domain-invariant mapping network,” in *Proceedings of the IEEE/CVF conference on Computer Vision and Pattern Recognition*, 2019, pp. 719–728.
- [39] A. Chakraborty, M. Alam, V. Dey, A. Chattopadhyay, and D. Mukhopadhyay, “Adversarial attacks and defences: A survey,” *arXiv preprint arXiv:1810.00069*, 2018.
- [40] S. Zhang, R. Ji, J. Hu, X. Lu, and X. Li, “Face sketch synthesis by multidomain adversarial learning,” *IEEE transactions on neural networks and learning systems*, vol. 30, no. 5, pp. 1419–1428, 2018.
- [41] J. Li, R. Ji, H. Liu, X. Hong, Y. Gao, and Q. Tian, “Universal perturbation attack against image retrieval,” in *Proceedings of the IEEE/CVF International Conference on Computer Vision*, 2019, pp. 4899–4908.
- [42] M. Sharif, S. Bhagavatula, L. Bauer, and M. K. Reiter, “Accessorize to a crime: Real and stealthy attacks on state-of-the-art face recognition,” in *Proceedings of the 2016 acm sigsac conference on computer and communications security*, 2016, pp. 1528–1540.
- [43] K. Eykholt, I. Evtimov, E. Fernandes, B. Li, A. Rahmati, C. Xiao, A. Prakash, T. Kohno, and D. Song, “Robust physical-world attacks on deep learning visual classification,” in *Proceedings of the IEEE conference on computer vision and pattern recognition*, 2018, pp. 1625–1634.
- [44] I. J. Goodfellow, J. Shlens, and C. Szegedy, “Explaining and harnessing adversarial examples,” *arXiv preprint arXiv:1412.6572*, 2014.
- [45] A. Kurakin, I. J. Goodfellow, and S. Bengio, “Adversarial examples in the physical world,” in *Artificial intelligence safety and security*, Chapman and Hall/CRC, 2018, pp. 99–112.
- [46] S.-M. Moosavi-Dezfooli, A. Fawzi, and P. Frossard, “Deepfool: A simple and accurate method to fool deep neural networks,” in *Proceedings of the IEEE conference on computer vision and pattern recognition*, 2016, pp. 2574–2582.
- [47] N. Narodytska and S. P. Kasiviswanathan, “Simple black-box adversarial perturbations for deep networks,” *arXiv preprint arXiv:1612.06299*, 2016.
- [48] C. Xiao, J.-Y. Zhu, B. Li, W. He, M. Liu, and D. Song, “Spatially transformed adversarial examples,” *arXiv preprint arXiv:1801.02612*, 2018.
- [49] G. Zhang, H. Zhang, Y. Chen, and Y. Zheng, “Close-set camera style distribution alignment for single camera person re-identification,” *Neurocomputing*, vol. 486, pp. 93–103, 2022.
- [50] Z. Gao, L. Gao, H. Zhang, Z. Cheng, R. Hong, and S. Chen, “Dcr: A unified framework for holistic/partial person reid,” *IEEE Transactions on Multimedia*, vol. 23, pp. 3332–3345, 2020.
- [51] Z. Zheng, L. Zheng, Y. Yang, and F. Wu, “Query attack via opposite-direction feature: Towards robust image retrieval,” *arXiv preprint arXiv:1809.02681*, 2018.
- [52] W. Hu and Y. Tan, “Generating adversarial malware examples for black-box attacks based on gan,” *arXiv preprint arXiv:1702.05983*, 2017.
- [53] W. Li, R. Zhao, T. Xiao, and X. Wang, “Deep-reid: Deep filter pairing neural network for person re-identification,” in *CVPR*, 2014, pp. 152–159.
- [54] L. Wei, S. Zhang, W. Gao, and Q. Tian, “Person transfer gan to bridge domain gap for person re-identification,” in *CVPR*, 2018, pp. 79–88.
- [55] X. Zhang, H. Luo, X. Fan, W. Xiang, Y. Sun, Q. Xiao, W. Jiang, C. Zhang, and J. Sun, “Alignedreid: Surpassing human-level performance in person re-identification,” *arXiv preprint arXiv:1711.08184*, 2017.
- [56] L. Zheng, Y. Yang, and A. G. Hauptmann, “Person re-identification: Past, present and future,” *arXiv preprint arXiv:1610.02984*, 2016.
- [57] X. Qian, Y. Fu, Y.-G. Jiang, T. Xiang, and X. Xue, “Multi-scale deep learning architectures for person re-identification,” in *ICCV*, 2017, pp. 5399–5408.
- [58] W. Li, X. Zhu, and S. Gong, “Harmonious attention network for person re-identification,” in *CVPR*, 2018, pp. 2285–2294.
- [59] Z. Zhong, L. Zheng, Z. Zheng, S. Li, and Y. Yang, “Camera style adaptation for person re-identification,” in *CVPR*, 2018, pp. 5157–5166.
- [60] W. Deng, L. Zheng, Q. Ye, G. Kang, Y. Yang, and J. Jiao, “Image-image domain adaptation with preserved self-similarity and domain-dissimilarity for person re-identification,” in *CVPR*, 2018, pp. 994–1003.
- [61] Z. Zheng, L. Zheng, and Y. Yang, “Unlabeled samples generated by gan improve the person re-identification baseline in vitro,” in *CVPR*, 2017, pp. 3754–3762.
- [62] Z. Zhong, L. Zheng, S. Li, and Y. Yang, “Generalizing a person retrieval model hetero-and homogeneously,” in *ECCV*, 2018, pp. 172–188.
- [63] A. Madry, A. Makelov, L. Schmidt, D. Tsipras, and A. Vladu, “Towards deep learning models resistant to adversarial attacks,” *arXiv preprint arXiv:1706.06083*, 2017.